



Cite this: *Nanoscale*, 2017, **9**, 18216

Received 6th September 2017,  
Accepted 6th November 2017

DOI: 10.1039/c7nr06645g

rsc.li/nanoscale

## Polycrystalline soft carbon semi-hollow microrods as anode for advanced K-ion full batteries†

Xuanpeng Wang,<sup>a</sup> Kang Han,<sup>a</sup> Dongdong Qin,<sup>a</sup> Qi Li,<sup>\*a</sup> Chenyang Wang,<sup>a</sup> Chaojiang Niu<sup>a</sup> and Liqiang Mai<sup>id</sup> <sup>\*a,b</sup>

**Soft carbon, which possesses the advantages of low cost and considerable potassium storage capacity, has been widely studied as an anode in K-ion batteries (KIBs). Herein, we constructed a novel polycrystalline semi-hollow microrods-structured soft carbon as an anode in KIBs, which exhibited both high capacity and excellent cycling stability.**

### 1. Introduction

Developing energy storage technology is an effective pathway for integrating renewable energy systems into the daily grid systems.<sup>1,2</sup> The electrochemical energy storage devices are the most promising candidates in energy storage systems, such as Li-ion batteries (LIBs), Na-ion batteries (NIBs), Zn-ion batteries (ZIBs), Al-ion batteries (AIBs) and Mg-ion batteries (MIBs).<sup>3–10</sup> Recently, K-ion batteries (KIBs) have received extensive attention due to their advantages of availability of abundant K-based materials and the similar output voltage to LIBs.<sup>11–22</sup> However, most of the KIB electrode materials suffer from low energy density and short cycling life-span due to the large size of K-ions.<sup>23–27</sup> Therefore, strategies to solve the above-mentioned issues are the hotspot and frontier of current research in KIBs. Nevertheless, in order to compete with the commercial graphite in LIBs, the cycling and rate performances of the carbon-based materials in KIBs need to be further improved. Generally, hollow structures were designed for enhancing the electrochemical performance in energy storage systems.<sup>28–35</sup> Hence, we hypothesize that the construction of hollow nanostructured soft carbon would significantly buffer the large volume expansion during potassiation/depotassiation, resulting in enhanced potassium storage properties particularly cycling stability.

Carbon-based anode materials such as graphite, hard carbon, graphene, soft carbon and hard-soft carbon composites have been widely investigated in KIBs, which can provide >300 mA h g<sup>-1</sup> capacity below 0.25 V vs. K/K<sup>+</sup> (similar to commercial graphite in LIBs).<sup>36–40</sup> However, these carbon-based anodes suffer from poor rate capacity and rapid capacity fading due to the large volume expansion of over 60% when forming KC<sub>8</sub> during potassiation.<sup>39</sup> To address the drawbacks of these KIBs anodes, Ji *et al.* conducted a series of studies on soft carbon and other carbon-based anodes.<sup>11,36,38,39</sup> They reported the electrochemical potassium-storage properties of soft carbon for the first time, and also confirmed that soft carbon exhibited superior cyclability and rate capacity compared to those of graphite.<sup>36</sup> Therefore, soft carbon is considered to be one of the most promising carbon-based anodes in KIBs with commercial prospects.<sup>41–43</sup> Nevertheless, in order to compete with the commercial graphite in LIBs, the cycling and rate performances need to be further improved.

Herein, a polycrystalline soft carbon semi-hollow microrods based anode, which is composed of numerous nanosheets and cavities, was constructed for use in KIBs. With a large electrode-electrolyte contact area, short K-ion diffusion distances and suitable hollow volume for potassium storage, the semi-hollow microrods manifested excellent electrochemical performances in KIBs (Scheme 1). Moreover, the advanced *in/ex situ* X-ray diffraction (XRD) test results revealed the regulating evolution of the interlayer spacing and the excellent reversibility between the crystalline and amorphous state of soft carbon during the potassiation/depotassiation processes. Further, the results demonstrated that the semi-hollow microrods could provide a stable framework structure and reversible crystal structure during the insertion/extraction processes of large-sized K-ions. As a result, the polycrystalline soft carbon semi-hollow microrods exhibit long cycling life-span, good rate capability and superior reversible capacity when tested as the KIB anode.

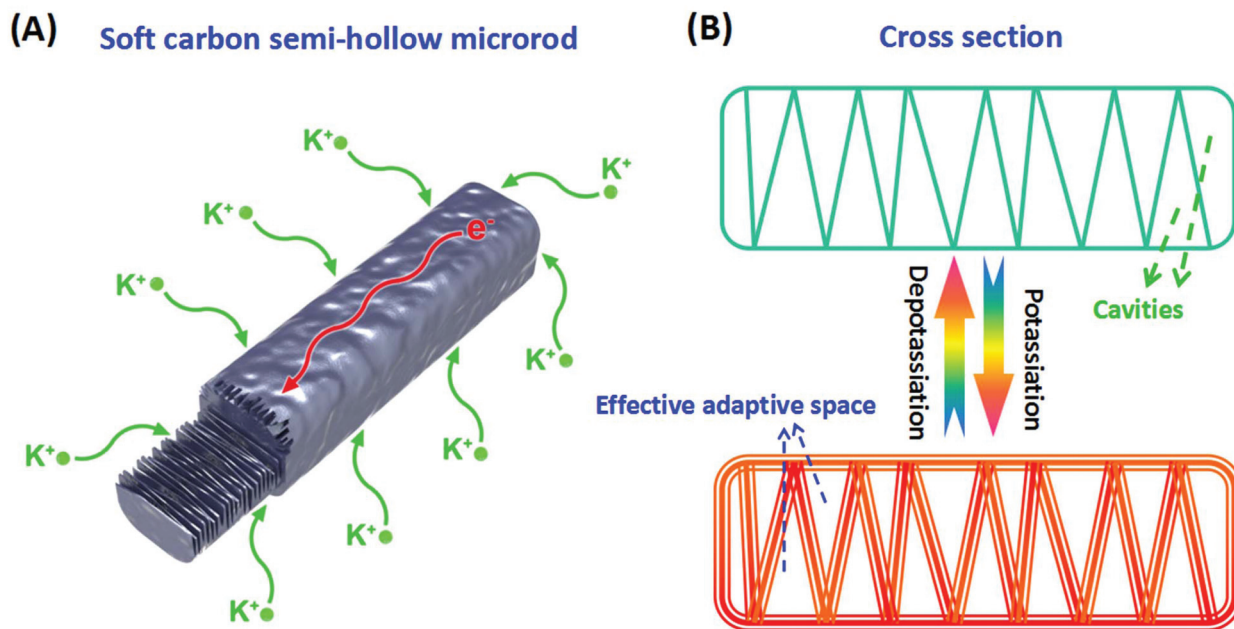
Furthermore, the K-ion full batteries based on polycrystalline soft carbon semi-hollow microrods and K<sub>0.6</sub>CoO<sub>2</sub> interconnected nanoparticles were assembled, manifesting good cycling stability and high reversible capacity. This study

<sup>a</sup>State Key Laboratory of Advanced Technology for Materials Synthesis and Processing, Wuhan University of Technology, Wuhan 430070, China.

E-mail: mlq518@whut.edu.cn, qi.li@whut.edu.cn

<sup>b</sup>Department of Chemistry, University of California, Berkeley, California 94720, USA

†Electronic supplementary information (ESI) available: SEM, FT-IR, Raman, BET, XRD, electrochemical properties. See DOI: 10.1039/c7nr06645g



**Scheme 1** (A, B) Schematic illustrations of the polycrystalline soft carbon semi-hollow microrod with large electrode–electrolyte contact area, short K-ion diffusion distances and reduced volume expansion during the K-ions insertion/extraction processes.

explores an unexploited field of carbon-based materials for K-ion full battery anodes, and could carve out an effective strategy for enhancing the cycling performance in potassium storage systems.

## 2. Experimental

### 2.1. Synthesis of soft carbon and $K_{0.6}CoO_2$

The soft carbon samples were prepared by pyrolysis of 3,4,9,10-perylenetetracarboxylic dianhydride (PTCDA, 98%, Alfa Aesar) at 800 °C, 900 °C and 1000 °C (5 °C min<sup>-1</sup>) for 10 h under flowing argon atmosphere. The  $K_{0.6}CoO_2$  interconnected nanoparticles were typically synthesized by a facile organic-acid-assisted method.<sup>15</sup> First, KOH (5.3 mmol),  $C_4H_6O_4Co \cdot 4H_2O$  (5.0 mmol) and citric acid (2.0 g) were dispersed in deionized water (40 mL) under vigorous stirring at 25 °C to obtain a red solution. Second, this solution was dried at 80 °C and baked at 160 °C for 12 h to obtain a loose sponge-like solid. Finally, the sponge-like solid was pre-sintered at 300 °C (5 °C min<sup>-1</sup>) for 2 h and then sintered under argon at 700 °C (5 °C min<sup>-1</sup>) in flowing  $O_2$  for 12 h to obtain  $K_{0.6}CoO_2$  interconnected nanoparticles.

### 2.2. Material characterization

*In situ* XRD experiments during electrochemical testing of battery was performed on a Bruker D8 Discover X-ray diffractometer with a non-monochromated Cu  $K\alpha$  X-ray source scanned at  $2\theta$  range of 19–29°. For *in situ* XRD measurement, the electrode was placed right behind an X-ray-transparent beryllium window, which also acts as a current collector. The *in situ* XRD signals were collected using the planar detector in

a still mode during the charge/discharge processes, and each pattern took 200 s to acquire. Anodes were obtained with 90% active material and 10% PTFE (using *N*-methyl-2-pyrrolidone solvent by weight). The reference electrode was K metal (99.5%, Sigma-Aldrich). A 0.8 M  $KPF_6$  solution in a mixed solvent of ethylene carbon/dimethyl carbonate (1 : 1 w/w, with 5 wt% FEC) was used as the electrolyte; a Whatman glass microfiber filter paper (grade GF/A) was used as the separator. The cathode was cut into square slices with an area of  $\sim 0.49$  cm<sup>2</sup> and a thickness of  $\sim 0.1$  mm. The mass loading of the active material was approximately 1.6–2.0 mg cm<sup>-2</sup>.

Powder XRD measurements were performed to obtain the crystallographic information using a Bruker D8 Discover X-ray diffractometer equipped with a non-monochromated Cu  $K\alpha$  X-ray source. Field-emission scanning electron microscopy (FESEM) images were collected using a JEOL-7100F microscope. Energy-dispersive X-ray spectroscopy (EDS) was performed using an Oxford EDS IE250. The Brunauer–Emmett–Teller (BET) surface area was calculated from nitrogen adsorption isotherms measured at 77 K using a Tristar-3020 instrument. Transmission electron microscopy (TEM) and high-resolution TEM were conducted on a JEOL JEM-2100F STEM/EDS microscope. FT-IR spectra were recorded using a Thermo Nicolet Nexus spectroscopy system. Raman spectra were recorded using a Renishaw INVIA micro-Raman spectroscopy system. The tap density and apparent density were tested by the Tap Density Tester (BT-301).

### 2.3. Electrochemical measurements

The electrochemical measurements were carried out using 2016 coin cells, which were assembled in a glove box filled

with pure argon gas. K metal (99.5%, Sigma-Aldrich) was used as the reference electrode, 0.8 M KPF<sub>6</sub> in a mixture of ethylene carbon/dimethyl carbonate (1 : 1 w/w, with 5 wt% FEC) was used as the electrolyte, and a Whatman glass microfiber filter (Grade GF/A) was used as the separator. Anodes were composed of 90% active material and 10% PTFE (using *N*-methyl-2-pyrrolidone as a solvent) by weight. Cathodes were obtained with 70% active material, 20% acetylene black and 10% PVDF (using *N*-methyl-2-pyrrolidone solvent by weight). The cathodes and anodes were cut into square slices  $\sim 0.49$  cm<sup>2</sup> in area and  $\sim 0.1$  mm in thickness. The loading of the anode and cathode materials are approximately 1.2–1.5 mg cm<sup>-2</sup> and 1.7–2.1 mg cm<sup>-2</sup>, respectively. The mass loading of the cathode is 1.4 times larger than that of the anode. Before assembling the half and full cells, the soft carbon electrode and metal potassium were placed together and 4–6 drops of electrolyte were added onto the soft carbon electrode plate and then placed in an argon-gas-filled glove box for 60–70 seconds. Galvanostatic charge/discharge tests of anode and cathode were performed over a potential range from 0.01 to 1.5 V and from 2.0 to 4.0 V vs. K<sup>+</sup>/K using a multichannel battery testing system (LAND CT2001A), respectively. The full cells were tested over a potential range of 0.8–3.5 V vs. K<sup>+</sup>/K using a multichannel battery testing system (LAND CT2001A). Cyclic voltammetry (CV) and electrochemical impedance spectra (EIS) were conducted using an electrochemical workstation (CHI600E and Autolab PGSTAT 302N).

### 3. Results and discussion

#### 3.1. Morphology and structural characterization

The soft carbon samples were prepared by direct pyrolysis of PTCDA at different temperatures under flowing argon atmosphere. XRD patterns of these three samples clearly exhibit

broadened (002) diffraction peaks, revealing an average *d*-spacing of  $\sim 0.36$  nm (Fig. 1A). The morphologies of these three soft carbon samples are presented in Fig. S1.† The scanning electron microscopy (SEM) images show that the obtained microrods are more uniform when sintered at 900 °C, compared with those at 800 °C and 1000 °C. The diameters of the individual microrods (900 °C) are in the range of 1.5–2.0 μm (Fig. 1B). Moreover, there are numerous nanosheets arranged in the interior of the microrods, and the distance between the two neighbouring nanosheets (with a thickness of  $\sim 48$  nm) is about 150–200 nm (Fig. 1C and D). TEM images of the microrod display a clear semi-hollow structure (Fig. 1E), with plenty of cavities included in the microrod (Fig. 1F), which is highly consistent with the SEM characterization results. The high-resolution TEM image vividly displays the disordered lattice fringes ( $\sim 0.36$  nm), demonstrating a typical turbostratic structure (Fig. 1G).<sup>36</sup> The corresponding selected area electron diffraction (SAED) pattern presents three evident halo rings, indicating a short-range order of the semi-hollow microrod soft carbon (Fig. 1H).<sup>42</sup> The FT-IR spectroscopy analyses show that the samples obtained at different temperatures have a similar valence bond structure (Fig. S2A†). Raman spectroscopy was also used to confirm the nature of the carbon in three samples, and the results are shown in Fig. S2B.† For all of the three samples, the intensity of the G-band is comparable to that of the D-band, verifying that the carbon possesses a certain degree of graphitization.<sup>44,45</sup> The specific surface area and pore size distribution of these three samples were measured by the BET, *t*-plot empirical law and BJH method. As shown in Fig. S3,† the BET results indicate that the soft carbon sintered at 900 °C exhibits the highest surface area (72 m<sup>2</sup> g<sup>-1</sup>) compared to that at 800 °C (48 m<sup>2</sup> g<sup>-1</sup>) and 1000 °C (54 m<sup>2</sup> g<sup>-1</sup>). The density test results infer that the tap density and apparent density of the soft carbon sintered at 900 °C are  $\sim 0.47$  g cm<sup>-3</sup> and  $\sim 0.42$  g cm<sup>-3</sup>, respectively (Fig. S4†).

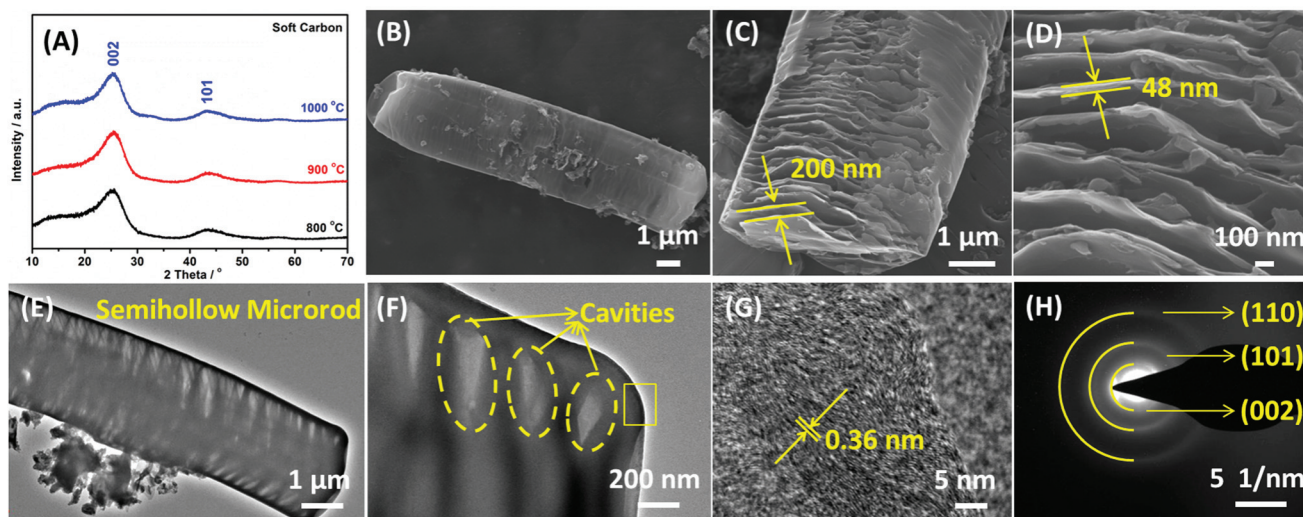


Fig. 1 XRD patterns (A) of soft carbon samples sintered at 800 °C, 900 °C and 1000 °C. SEM images (B–D), TEM images (E, F), high-resolution TEM image (G) and SAED pattern (H) of soft carbon semi-hollow microrods sintered at 900 °C.

### 3.2. Potassium storage mechanism

To study the potassium storage mechanism of the soft carbon in KIBs, *in/ex situ* experiments were conducted (Fig. 2 and Fig. S5†). The structural evolutions of the soft carbon during K-ion insertion/extraction under *in situ* XRD testing is shown in Fig. 2A. The broad peak located at  $24^\circ$  belonging to the (002) plane of soft carbon, which is the characteristic peak, indicates highly reversible features during the electrochemical processes. The additional characteristic peak located at  $24.7^\circ$  could be attributed to the binder material.<sup>36,46</sup> Upon the initial potassiation process, the (002) peak shifts toward lower angle, then weakens and gradually disappears, indicating the increased interplanar spacing and the transformation of the crystalline to the amorphous state.<sup>42</sup> Interestingly, the (002) peak re-appears, strengthens and shifts to a higher angle, when charged to 1.5 V in the subsequent depotassiation process. In short, the *d*-spacing of the (002) plane increases with the insertion of K-ions ( $D_2 > D_1$ ) and decreases with the extraction of K-ions ( $D_2 > D_3$ ) (Fig. 2B). Moreover, the soft carbon reversibly converts between crystalline and amorphous states during the potassiation/depotassiation processes.<sup>46</sup> A similar behaviour is also observed in the subsequent cycles. The same phenomenon was also observed in *ex situ* XRD tests, which further confirmed that the interplanar spacing of soft carbon can provide reversible potassium storage sites (Fig. S5†). On the basis of *in/ex situ* XRD analyses, the potassium storage mechanism was clearly revealed and strongly confirmed the highly reversible property of soft carbon during electrochemical potassium storage process.<sup>23,44</sup>

### 3.3. Potassium storage performance in half cells

The synthesized soft carbon samples sintered at different temperatures were tested as anodes in KIBs. In the case of the

microrod samples, the sample sintered at  $900^\circ\text{C}$  exhibits the best potassium storage performance, which could be attributed to the more uniform morphology structure, suitable graphitization degree and highest surface area compared with the other two samples (Fig. S6 and Fig. S7†). Therefore,  $900^\circ\text{C}$  was considered as the optimized sintering condition for semi-hollow microrods. The cyclic voltammetry (CV) curves for semi-hollow microrods display one pair of cathodic/anodic peaks (0.37/0.50 V) during the first electrochemical process (Fig. 3A). The large irreversible peak located at 0.37 V is attributed to the formation of the solid-electrolyte interphase (SEI) and the inactivation of the inserted potassium sites.<sup>37,41</sup> Clearly, the following two CV curves exhibit similar characteristics, indicating the same reaction mechanism and reversibility of K-ions insertion/extraction. The semi-hollow microrods manifest excellent cycling stability and rate capability. At a current density of  $100\text{ mA g}^{-1}$ , the semi-hollow microrods delivered an initial discharge capacity of  $599\text{ mA h g}^{-1}$ . The discharge capacity was maintained at  $312\text{ mA h g}^{-1}$  in the second cycle, which is very close to its theoretical capacity, and retained  $249\text{ mA h g}^{-1}$  after 100 cycles (corresponding to a capacity retention rate of 80%, relative to the second cycle) (Fig. 3B). Representative potassiation/depotassiation curves of soft carbon semi-hollow microrods at  $100\text{ mA g}^{-1}$  are presented in Fig. 3C, which show similar potassiation/depotassiation behaviour after initial cycles, manifesting excellent cycling stability. The Nyquist plots and *ex situ* SEM images of semi-hollow microrods before and after cycling are shown in Fig. S8 and S9;† these data indicate that microrods still possess a stable framework structures after long cycling.

When tested at various current densities ranging from 100 to  $1000\text{ mA g}^{-1}$  and then back to  $100\text{ mA g}^{-1}$ , the semi-hollow microrods exhibit a high discharge capacity and superior rate stability, demonstrating a prominent rate performance

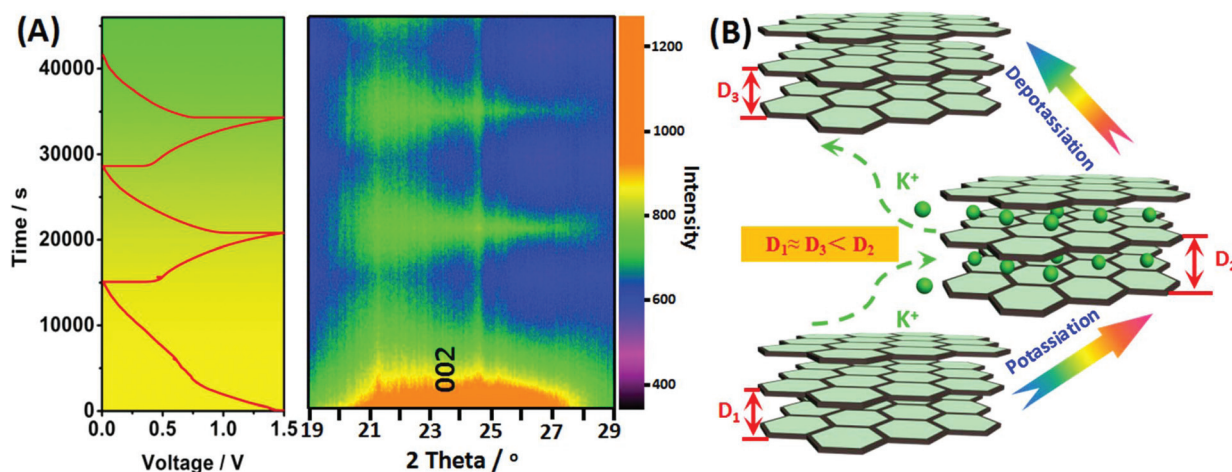


**Fig. 2** Potassium storage mechanism of soft carbon semi-hollow microrods ( $900^\circ\text{C}$ ). (A) *In situ* XRD patterns of soft carbon semi-hollow microrods during galvanostatic depotassiation/potassiation at  $100\text{ mA g}^{-1}$ . The image plot of the diffraction patterns at  $19\text{--}29^\circ$  during the first two cycles. The horizontal axis represents the selected  $2\theta$  regions, and time is on the vertical axis. The diffraction intensity is colour coded with the scale bar shown on right. The corresponding voltage curve is plotted to the left. (B) Schematic illustration of the evolution for (002) interplanar spacing in soft carbon.

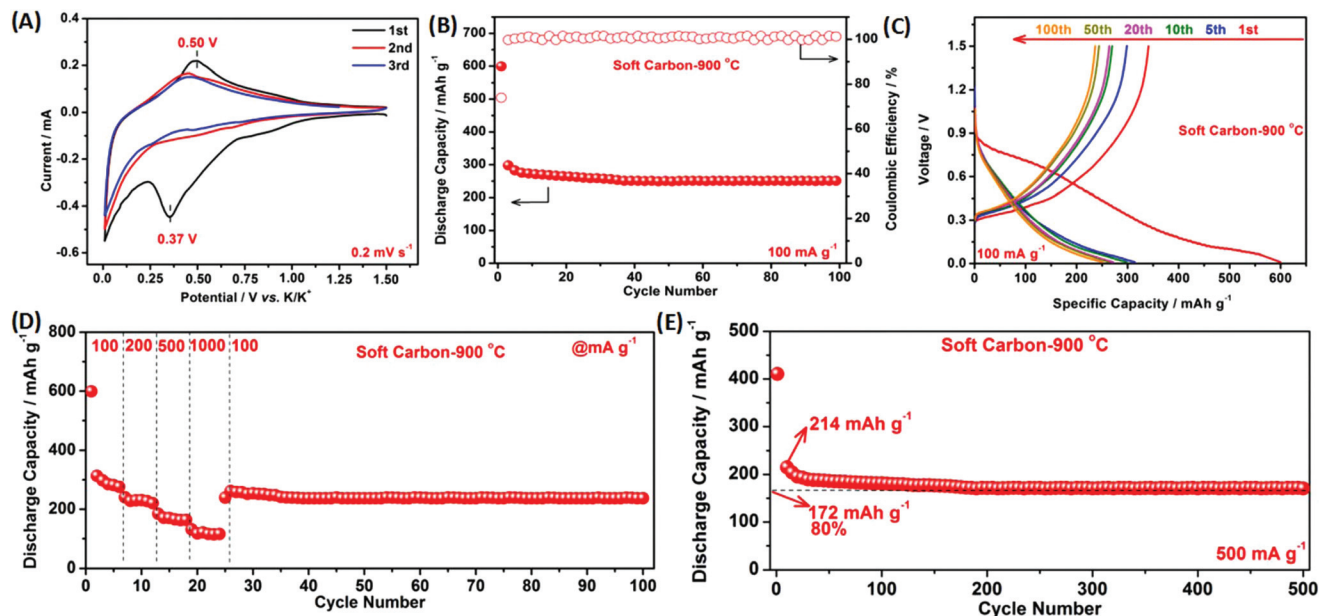


**Fig. 3** Characterization of electrochemical performance for soft carbon semi-hollow microrods sintered at 900 °C in KIBs. (A) Cyclic voltammograms at a scan rate of 0.2 mV s<sup>-1</sup> over the potential window of 0.01–1.5 V vs. K<sup>+</sup>/K. (B) Cyclic performance tested at a current density of 100 mA g<sup>-1</sup>. (C) Depotassiation/potassiation curves tested at 100 mA g<sup>-1</sup>. (D) Rate performance at various rates ranging from 100, 200, 500, 1000 mA g<sup>-1</sup> back to 100 mA g<sup>-1</sup>. (E) Long-life cycling performance measured at 500 mA g<sup>-1</sup>.

(Fig. 3D). When the current density is returned to 100 mA g<sup>-1</sup>, ~94% of the discharge capacity can be recovered and the capacity remains stable for 100 cycles with no significant capacity fading. The most appealing property of the semi-hollow microrods is their excellent cycling stability at a high rate. When tested at a high rate of 500 mA g<sup>-1</sup>, ~82% of the

2<sup>nd</sup> discharge capacity can be retained after 500 cycles (Fig. 3E). To the best of our knowledge, our as-prepared semi-hollow microrods-based soft carbon anode materials exhibit the best electrochemical performance among KIB carbon-based anodes in terms of discharge capacity, stability and rate performance (Table S1†).

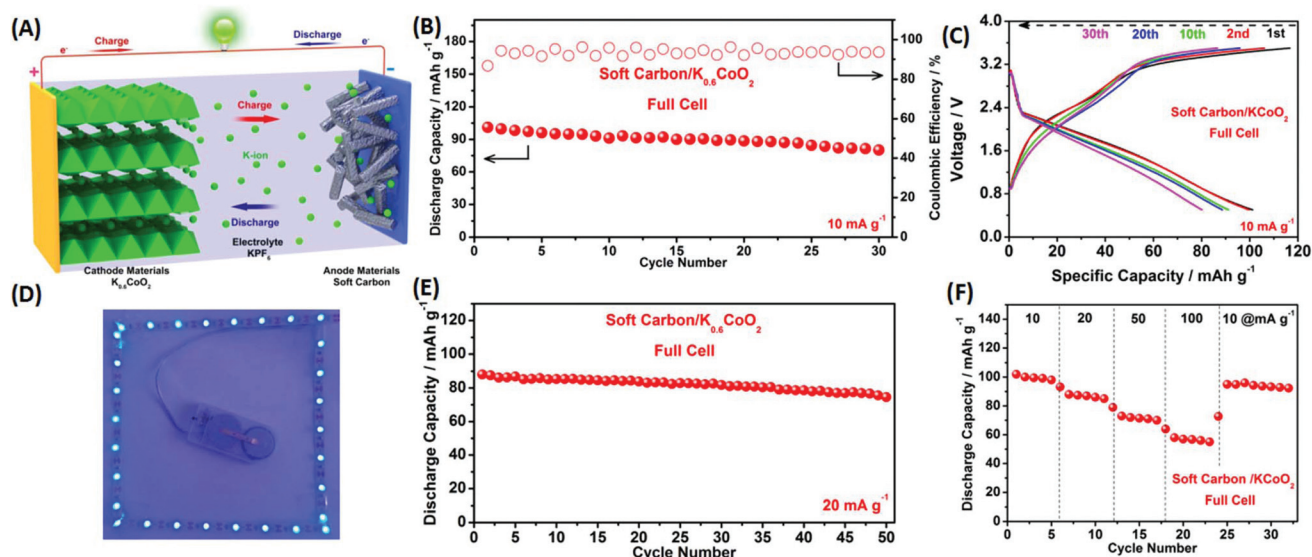


**Fig. 4** Schematic illustration and electrochemical performance of the full cell based on soft carbon semi-hollow microrods/K<sub>0.6</sub>CoO<sub>2</sub> interconnected nanoparticles. (A) Schematic illustration of the K-ion full battery and the corresponding Coulombic efficiency at a current density of 10 mA g<sup>-1</sup>. (C) The lighted LED belts driven. (D) Cycling performance and the corresponding Coulombic efficiency at current density of 20 mA g<sup>-1</sup>.

### 3.4. Potassium storage performance in full cells

The K-ion full cells based on soft carbon semi-hollow microrods,  $K_{0.6}CoO_2$  interconnected nanoparticles and electrolyte (0.8 M KPF<sub>6</sub>) were also fabricated. Before full cell assembly, the XRD, SEM, TEM and electrochemical property characterizations of  $K_{0.6}CoO_2$  interconnected nanoparticles were conducted (Fig. S10–S13†). Fig. 4A displays the schematic of the K-ion conduction between soft carbon and  $K_{0.6}CoO_2$  during the K-ion insertion/extraction. The corresponding lighted LED belts indicate that our as-prepared full cell can work effectively after being fully charged (Fig. 4D). As shown in Fig. 4B and C, the full cell delivers an initial discharge capacity of 101 mA h g<sup>-1</sup> (based on the mass of anode) at a current density of 10 mA g<sup>-1</sup>, maintaining 81 mA h g<sup>-1</sup> after 50 cycles (capacity retention rate is ~80%). The initial Coulombic efficiency is ~86.7%, and reaches ~93% in the following cycles. Notably, when tested at a current density of 20 mA g<sup>-1</sup>, ~84% of the initial capacity can be retained after 50 cycles (Fig. 4D). As the current density increases from 10 to 20, 50, and 100 mA g<sup>-1</sup>, the full cell shows an average capacity of 100, 87, 72 and 57 mA h g<sup>-1</sup>, respectively (Fig. 4F), manifesting high rate performance in K-ion full batteries.

The remarkable potassium storage performance of the soft carbon semi-hollow microrods can be attributed to their unique semi-hollow structure and low crystallinity disordered features. First, the semi-hollow nanostructure possesses enough space to accommodate volume expansion (Scheme 1 and Fig. 1C, E), which is beneficial to the cycling stability. Second, the unique structure can provide a large electrode-electrolyte contact area and shorten the K-ion diffusion distances, resulting in high rate performance. Third, the low crystallinity and typical turbostratic structure offer more reversible potassium storage active sites (Fig. 2), and further boost the electrochemical reaction kinetics. By combining all the above advantages, the soft carbon semi-hollow microrods demonstrate impressive electrochemical performances with exceptional capacity and outstanding cycling stability in K-ion full batteries.

## 4. Conclusions

In summary, we have demonstrated that soft carbon semi-hollow microrods represent promising anode materials for high performance KIBs. A high initial discharge capacity of 314 mA h g<sup>-1</sup> is achieved and 249 mA h g<sup>-1</sup> is retained after 100 cycles when tested for KIBs. Moreover, the full cell based on soft carbon semi-hollow microrods and  $K_{0.6}CoO_2$  interconnected nanoparticles exhibits a capacity of 101 mA h g<sup>-1</sup> at a current density of 10 mA g<sup>-1</sup>, and it undergoes stable charge/discharge process for 50 cycles. On the basis of *in/ex situ* XRD analysis and electrochemical characterizations, we have confirmed that soft carbon semi-hollow microrods can provide suitable hollow space to alleviate volume expansion during potassiation/depotassiation processes, which is attributed to the high discharge capacity and excellent cycling stability

when used as K-ion full battery anode. Our study highlights that designing and constructing hollow nanostructures with a stable structure is an effective approach for improving the cycling stability of K-ion full batteries.

## Conflicts of interest

There are no conflicts to declare.

## Acknowledgements

This work was supported by the National Key Research and Development Program of China (2016YFA0202603), the National Basic Research Program of China (2013CB934103), the Programme of Introducing Talents of Discipline to Universities (B17034), the National Natural Science Foundation of China (51521001), the National Natural Science Fund for Distinguished Young Scholars (51425204), and the Fundamental Research Funds for the Central Universities (WUT: 2016III001, 2017IVA096, 2017IVA100, 2017III009, 2017III040), State Key Laboratory of Advanced Technology for Materials Synthesis and Processing (WUT: 2017-KF-2), the National Students Innovation and Entrepreneurship Training Program (WUT: 20171049701013). Prof. Liqiang Mai gratefully acknowledged financial support from China Scholarship Council (No. 201606955096). We thank Prof. Peidong Yang of University of California, Berkeley for strong support and stimulating discussions.

## Notes and references

- V. Palomares, P. Serras, I. Villaluenga, K. B. Hueso, J. Carretero-González and T. Rojo, *Energy Environ. Sci.*, 2012, **5**, 5884–5901.
- J. W. Choi and D. Aurbach, *Nat. Rev. Mater.*, 2016, **1**, 16013.
- B. Dunn and J. M. Tarascon, *Science*, 2011, **334**, 928–935.
- M. Armand and J. M. Tarascon, *Nature*, 2008, **451**, 652–657.
- D. Kundu, B. D. Adams, V. Duffort, S. H. Vajargah and L. F. Nazar, *Nat. Energy*, 2016, **1**, 16119.
- H. Pan, Y. Shao, P. Yan, Y. Cheng, K. S. Han, Z. Nie, C. Wang, J. Yang, X. Li and P. Bhattacharya, *Nat. Energy*, 2016, **1**, 16039.
- X. Zhang, Y. Tang, F. Zhang and C. S. Lee, *Adv. Energy Mater.*, 2016, **6**, 1502588.
- M. C. Lin, M. Gong, B. Lu, Y. Wu, D. Y. Wang, M. Guan, M. Angell, C. Chen, J. Yang and B. J. Hwang, *Nature*, 2015, **520**, 325–328.
- Y. Shao, N. N. Rajput, J. Hu, M. Hu, T. Liu, Z. Wei, M. Gu, X. Deng, S. Xu and K. S. Han, *Nano Energy*, 2015, **12**, 750–759.
- Y. Shao, M. Gu, X. Li, Z. Nie, P. Zuo, G. Li, T. Liu, J. Xiao, Y. Cheng and C. Wang, *Nano Lett.*, 2014, **14**, 255–260.
- A. Eftekhari, Z. Jian and X. Ji, *ACS Appl. Mater. Interfaces*, 2016, **9**, 4404–4419.

- 12 L. Xue, Y. Li, H. Gao, W. Zhou, X. Lü, W. Kaveevitvichai, A. Manthiram and J. B. Goodenough, *J. Am. Chem. Soc.*, 2017, **139**, 2164–2167.
- 13 J. C. Pramudita, D. Sehrawat, D. Goonetilleke and N. Sharma, *Adv. Energy Mater.*, 2017, DOI: 10.1002/aenm.201700098.
- 14 Q. Zhao, J. Wang, Y. Lu, Y. Li, G. Liang and J. Chen, *Angew. Chem., Int. Ed.*, 2016, **55**, 12528–12532.
- 15 Y. Hironaka, K. Kubota and S. Komaba, *Chem. Commun.*, 2017, **53**, 8588–8591.
- 16 Q. Deng, J. Pei, C. Fan, J. Ma, B. Cao, C. Li, Y. Jin, L. Wang and J. Li, *Nano Energy*, 2017, **33**, 350–355.
- 17 H. Kim, J. C. Kim, S. H. Bo, T. Shi, D. H. Kwon and G. Ceder, *Adv. Energy Mater.*, 2017, **7**, 1700098.
- 18 W. Zhang, J. Mao, S. Li, Z. Chen and Z. Guo, *J. Am. Chem. Soc.*, 2017, **139**, 3316–3319.
- 19 Y. Liu, Z. Tai, Q. Zhang, H. Wang, W. K. Pang, H. K. Liu, K. Konstantinov and Z. Guo, *Nano Energy*, 2017, **35**, 36–43.
- 20 H. Gao, T. Zhou, Y. Zheng, Q. Zhang, Y. Liu, J. Chen, H. Liu and Z. Guo, *Adv. Funct. Mater.*, 2017, **27**, 1702634.
- 21 S. Chong, Y. Z. Chen, Y. Zheng, Q. Tan, C. Shu, Y. Liu, Z. Guo, S. Chong, Y. Z. Chen and Y. Zheng, *J. Mater. Chem. A*, 2017, **5**, 22465–22471.
- 22 Z. Tai, Y. Liu, Q. Zhang, T. Zhou, Z. Guo, H. K. Liu and S. X. Dou, *Green Energy Environ.*, 2017, DOI: 10.1016/j. gee.2017.04.002.
- 23 X. Wang, X. Xu, C. Niu, J. Meng, M. Huang, X. Liu, Z. Liu and L. Mai, *Nano Lett.*, 2017, **17**, 544–550.
- 24 X. Jiang, T. Zhang, L. Yang, G. Li and J. Y. Lee, *ChemElectroChem*, 2017, **4**, 2237–2242.
- 25 C. D. Wessells, S. V. Peddada, R. A. Huggins and Y. Cui, *Nano Lett.*, 2011, **11**, 5421–5425.
- 26 P. Padigi, J. Thiebes, M. Swan, G. Goncher, D. Evans and R. Solanki, *Electrochim. Acta*, 2015, **166**, 32–39.
- 27 Y. Chen, W. Luo, M. Carter, L. Zhou, J. Dai, K. Fu, S. Lacey, T. Li, J. Wan, X. Han, Y. Bao and L. Hu, *Nano Energy*, 2015, **18**, 205–211.
- 28 C. Niu, J. Meng, X. Wang, C. Han, M. Yan, K. Zhao, X. Xu, W. Ren, Y. Zhao, L. Xu, Q. Zhang, D. Zhao and L. Mai, *Nat. Commun.*, 2015, **6**, 7402.
- 29 L. Zhou, Z. Zhuang, H. Zhao, M. Lin, D. Zhao and L. Mai, *Adv. Mater.*, 2017, **29**, 1602914.
- 30 L. Yu, H. B. Wu and X. W. Lou, *Acc. Chem. Res.*, 2017, **50**, 293–301.
- 31 L. Yu, H. Hu, H. B. Wu and X. W. Lou, *Adv. Mater.*, 2017, **29**, 1604563.
- 32 Y. Liu, L. Yu, Y. Hu, C. Guo, F. Zhang and D. L. X. Wen, *Nanoscale*, 2012, **4**, 183–187.
- 33 S. Ding, D. Zhang, H. B. Wu, Z. Zhang and X. W. Lou, *Nanoscale*, 2012, **4**, 3651–3654.
- 34 X. Zhou, L. Yu and X. W. Lou, *Nanoscale*, 2016, **8**, 8384–8389.
- 35 D. Zhang, W. Sun, Y. Zhang, Y. Dou, Y. Jiang and S. X. Dou, *Adv. Funct. Mater.*, 2016, **26**, 7479–7485.
- 36 Z. Jian, W. Luo and X. Ji, *J. Am. Chem. Soc.*, 2015, **137**, 11566–11569.
- 37 W. Luo, J. Wan, B. Ozdemir, W. Bao, Y. Chen, J. Dai, H. Lin, Y. Xu, F. Gu and V. Barone, *Nano Lett.*, 2015, **15**, 7671–7677.
- 38 Z. Xing, Y. Qi, Z. Jian and X. Ji, *ACS Appl. Mater. Interfaces*, 2017, **9**, 4343–4351.
- 39 Z. Jian, S. Hwang, Z. Li, A. S. Hernandez, X. Wang, Z. Xing, D. Su and X. Ji, *Adv. Funct. Mater.*, 2017, **27**, 1700324.
- 40 X. Bie, K. Kubota, T. Hosaka, K. Chihara and S. Komaba, *J. Mater. Chem. A*, 2017, **5**, 4325–4330.
- 41 L. Wei, Z. Jian, Z. Xing, W. Wei, C. Bommier, M. Lerner and X. Ji, *ACS Cent. Sci.*, 2015, **1**, 516–522.
- 42 L. Fan, Q. Liu, S. Chen, Z. Xu and B. Lu, *Adv. Energy Mater.*, 2017, **5**, 4325–4330.
- 43 X. Wu, D. P. Leonard and X. Ji, *Chem. Mater.*, 2017, **29**, 5031–5042.
- 44 X. Wang, C. Niu, J. Meng, P. Hu, X. Xu, X. Wei, L. Zhou, K. Zhao, W. Luo and M. Yan, *Adv. Energy Mater.*, 2015, **5**, 1500716.
- 45 X. Wang, P. Hu, C. Niu, J. Meng, X. Xu, X. Wei, C. Tang, W. Luo, L. Zhou, Q. An and L. Mai, *Nano Energy*, 2017, **35**, 71–78.
- 46 S. Komaba, T. Hasegawa, M. Dahbi and K. Kubota, *Electrochem. Commun.*, 2015, **60**, 172–175.